PLEASE COMPLETE THE PUBLICATION FEE CONSENT FORM BELOW
AND
RETURN TO THE PRODUCTION EDITOR WITH YOUR PROOF CORRECTIONS

Please return this completed form and direct any questions to the Wiley Journal Production Editor at JGRAprod@wiley.com.

To order OnlineOpen, you must complete the OnlineOpen order form at:
https://authorservices.wiley.com/bauthor/onlineopen_order.asp
Authors who select OnlineOpen will be charged the standard OnlineOpen fee for your journal, but excess publication fees will still apply, if applicable. **If your paper has generated excess publication fees, please complete and return the form below in addition to completing the OnlineOpen order form online (excess fees are billed separately)**. If you would like to choose OnlineOpen and you have not already submitted your order online, please do so now.

YOUR ARTICLE DETAILS

Journal: *Journal of Geophysical Research: Space Physics*

Article: Shklyar, D. R., Manninen, J., Titova, E. E., Santolík, O., Kolmašová, I., & Turunen, T. (2020). Ground and space signatures of VLF noise suppression by whistlers. *Journal of Geophysical Research: Space Physics, 125,* 1–14. https://doi.org/10.1029/2019JA027430

OnlineOpen: No **Words:** 5,481 **Tables:** 0 **Figures:** 8 **Total Publishing Units:**19

Journal Base Fee:		$1,000
Excess Publishing Units:	0@$125	$0
Publication Fee Total:	USD	$1,000

An invoice will be mailed to the address you have provided once your edited article publishes online in its final format. Please include on this publication fee form any information that must be included on the invoice.

Publication Fees and Length Guidelines:
http://publications.agu.org/author-resource-center/

Frequently Asked Billing Questions:
http://onlinelibrary.wiley.com/journal/10.1002/(ISSN)2169-8996/homepage/billing_faqs.pdf

Purchase Order Instructions:
Wiley must be listed as the contractor on purchase orders to prevent delay in processing invoices and payments.

WILEY

Author Query Form

Journal: Journal of Geophysical Research: Space Physics

Article: jgra55531

Dear Author,

During the copyediting of your manuscript the following queries arose.

Please refer to the query reference call out numbers in the page proofs and respond to each by marking the necessary comments using the PDF annotation tools.

Please remember illegible or unclear comments and corrections may delay publication.

Many thanks for your assistance.

Query No.	Query	Remarks
Q1	AUTHOR: Per AGU style, abbreviations are to be avoided in the article title, unless defined in the abstract. Please modify accordingly.	
Q2	AUTHOR: Please verify that the linked ORCID identifiers are correct for each author	
Q3	AUTHOR: Please confirm that given names (Blue) and surnames/family names (Vermilion) have been identified correctly.	
Q4	AUTHOR: Please complete the Publication Fee Consent Form included with your article and return to the Production Editor with your proofs.	
Q5	AUTHOR: Please provide department for affiliation “National Research University Higher School of Economics”.	
Q6	AUTHOR: Please check that authors' affiliations are correct.	
Q7	AUTHOR: Please define VLF at first mention in the abstract if it is an acronym.	
Q8	AUTHOR: As per AGU guide, key points should be in complete sentence; hence, please check changes made in the first key point if appropriate.	
Q9	AUTHOR: Please define VLF at first mention in the text if it is an acronym.	

Please confirm that the funding sponsor list below was correctly extracted from your article: that it includes all funders and that the text has been matched to the correct FundRef Registry organization names. If a name was not found in the FundRef registry, it may not be the canonical name form, it may be a program name rather than an organization name, or it may be an organization not yet included in FundRef Registry. If you know of another name form or a parent organization name for a “not found” item on this list below, please share that information.

FundRef name	FundRef Organization Name
Academy of sciences of Finland	not found
Grantová Agentura České Republiky (GACR)	not found
LTAUSA	not found
Russian Foundation for Basic Research (RFBR)	Russian Foundation for Basic Research

SPi | Journal Code: J G R A | Article ID 55531 | Dispatch: 00.00.00 | CE: SCBV | No. of Pages: 14 | ME:

JGR Space Physics

RESEARCH ARTICLE
10.1029/2019JA027430

Ground and Space Signatures of VLF Noise Suppression by Whistlers

D. R. Shklyar[1,2], J. Manninen[3], E. E. Titova[1,4], O. Santolik[5,6], I. Kolmašová[5,6], and T. Turunen[3]

[1]Space Research Institute, Russian Academy of Sciences, Moscow, Russia, [2]National Research University Higher School of Economics, Moscow, Russia, [3]Sodankylä Geophysical Observatory, Sodankylä, Finland, [4]Polar Geophysical Institute, Murmansk, Russia, [5]Department of Space Physics, Institute of Atmospheric Physics, Czech Academy of Sciences, Prague, Czechia, [6]Faculty of Mathematics and Physics, Charles University, Prague, Czechia

Key Points:
- The first investigation of VLF noise suppression by multihop whistlers is based on wave and energetic particle measurements of Van Allen Probes
- Noise suppression by multihop whistler train is due to whistler-related modification of electron distribution in the noise generation region
- Electron phase space diffusion is investigated with the account of frequency and wave vector variations in the causative whistler train

Supporting Information:
- Supporting Information S1

Correspondence to:
J. Manninen,
Jyrki.Manninen@sgo.fi

Citation:
Shklyar, D. R., Manninen, J., Titova, E. E., Santolík, O., Kolmašová, I., & Turunen, T. (2020). Ground and space signatures of VLF noise suppression by whistlers. *Journal of Geophysical Research: Space Physics*, *125*, e2019JA027430. https://doi.org/10.1029/2019JA027430

Received 18 SEP 2019
Accepted 1 FEB 2020
Accepted article online 6 FEB 2020

Abstract VLF spectrograms registered at Kannuslehto ground station, after cleaning them from strong sferics, reveal VLF noise suppression by whistlers and whistler echo trains, which consists in significant reduction in the noise spectral power after a strong whistler event. We have found similar effect in the VLF data from Van Allen Probe B taken in the equatorial region on L-shell ~3. Detailed analysis of the data shows that the whistler echo train and the VLF noise have small wave normal angles. Based on this observation, we limit our analysis to parallel (ducted) whistler wave propagation. The persistence of whistler echo train, as well as the VLF noise, suggests that in the events under discussion, plasma is unstable in the frequency range corresponding to the observed VLF noise band. In an attempt to explain the effect of VLF noise suppression, we follow up the long-standing idea that relates this effect to the reduction of free energy in the unstable plasma distribution by whistler echo train. To develop this idea into qualitative model, we have studied the motion of energetic electrons, responsible for the noise generation, in the field of ducted whistler echo train. We show that energetic electrons that make the main contribution to the growth rate of VLF noise, during their bounce oscillations in the magnetosphere, are subject to multiple resonant impacts from the whistler echo train. These lead to energetic electron diffusion in the phase space and the corresponding reduction in free energy of the unstable distribution.

1. Introduction

In this paper we investigate the wave phenomenon in VLF frequency band which consists in transient reduction in the amplitude of VLF noise observed, first on the ground, after receiving a strong whistler. An example of this phenomenon is shown in Figure 1, which displays the spectrogram in the frequency band up to 8 kHz registered at Kannuslehto ground station in North Finland ($L = 5.5$) on 25 December 2011. The upper panel shows the wave magnetic field power spectral density over a 4 min interval. A significant decrease in spectral amplitude of VLF noise after receiving a strong whistler is clearly visible. We will turn our attention to other panels of Figure 1 later on. Other examples of VLF noise suppression by strong whistler echo trains, registered at Kannuslehto ground station, may be found in the supporting information of the paper.

Suppression effect under discussion was known for a long time. Based on observations on Siple Station, Helliwell et al. (1980) reported one-to-one correlation between hiss and optical emission (λ4278) intensity reductions immediately following each discrete VLF event. Since optical emission was assumed to result from particle precipitation, the authors suggested that both the hiss and optical emission reductions were caused by pitch angle scattering of energetic electrons by whistlers.

A comprehensive study of whistler induced suppression of VLF noise has been performed by Gail and Carpenter (1984). The authors have established several important features of the suppression effect; in particular, they demonstrated that the effect usually occurs when the driving whistler exhibits echoes confined to the frequency band occupied by the suppressed noise. They have also shown that the recovery of the noise band to the pre-event level takes several seconds, and this time correlates with the damping rate of the echo train. The effect of suppression of the VLF noise band produced by the whistler that triggered it has been reported by Platino et al. (2005) basing on observations by the Cluster spacecraft.

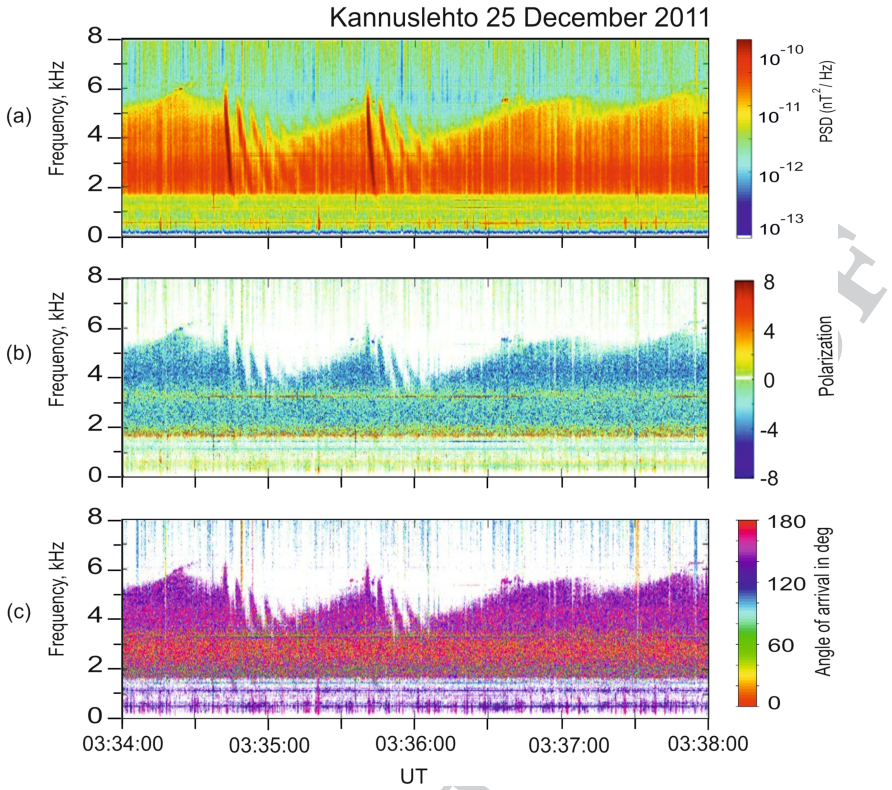

Figure 1. An example of spectrogram, obtained from ground station data, illustrating whistler induced suppression of VLF noise. (a) Logarithm of the total magnetic field power spectral density. (b) Parameter characterizing the wave polarization (see the text). (c) The angle between minor axis of the wave polarization ellipse and the north-south direction.

The explanation of the noise suppression suggested by Helliwell et al. (1980) and accepted by Gail and Carpenter (1984) consists in pitch angle scattering of energetic electrons by the whistler signal that leads to disruption of wave amplification in the magnetospheric interaction region. Those electrons which are scattered into the loss cone are observed as precipitation, providing the correlation between λ4278 optical emission and VLF noise suppression. We should mention that, although the pitch angle scattering may lead to reduction in the particle pitch angle anisotropy and, thus, decrease the amplification efficiency, the electrons close to the loss cone do not contribute significantly to the noise amplification due to small amplitude of interaction between these particles and parallel-propagating whistler waves.

2. Experimental Features of Suppression Phenomenon

2.1. Ground-Based Observations

Let us return to Figure 1 which presents the observations of VLF noise suppression by whistlers performed at Kannuslehto ground station (KAN) in Finland (67.74°N, 26.27°E; $L = 5.5$) on 25 December 2011. As was mentioned above, the upper panel displays the power spectral density of the wave magnetic field and illustrates the phenomenon under discussion. This spectrogram was preliminary cleaned from sferics using the method described in Manninen et al. (2016). Pay attention that a pronounced decrease in the noise intensity is observed after the second dispersed trace of the whistler echo train. Only the frequency band up to 8 kHz is displayed, although VLF emissions were recorded in the frequency range from 0.2 to 39 kHz. Magnetic field measurements were performed using two mutually orthogonal magnetic loop antennas oriented in the geographical north-south and east-west directions. This allows us to determine the polarization of waves which is characterized by the parameter p:

$$p = 10 \cdot \log_{10}\left(\frac{|H_R|^2}{|H_L|^2}\right), \quad (1)$$

where $H_{R,L} = (H_N \pm iH_E)/\sqrt{2}$ are the right- and left-hand polarized horizontal magnetic field components, respectively, and $H_{N,E}$ are the northward and eastward projections of the wave magnetic field. This parameter, displayed in the middle panel of Figure 1, shows that both whistlers and VLF noise have left-hand polarization, which indicates that the signals come to the Kannuslehto station over the Earth-ionosphere waveguide (Ostapenko et al., 2010). The lower panel of Figure 1 displays the angle (with an ambiguity of 180°) between the minor axis of the wave polarization ellipse and the north-south direction, which determines (with the same ambiguity) the direction of wave arrival at the station. Close values of the displayed quantity for both whistlers and noise suggest that they have close exit regions from the ionosphere. As for time characteristics of the noise suppression phenomenon, it becomes the most pronounced about 15–30 s after strong whistler event and lasts several tens of seconds.

2.2. Space Observations Onboard Van Allen Probes

We have not found suppression events in Cluster or RBSP data simultaneous with any one observed at Kannuslehto ground station. An independent suppression event that we have found in RBSP-B data is discussed below.

Intense whistlers and echo trains were registered onboard RBSP-B on 22 December 2014. VLF spectrogram up to 12 kHz obtained from magnetic (a) and electric (b) field measurements of the EMFISIS instrument (Kletzing et al., 2013) during the time period 19:23:53–19:24:17 UT when the instrument operated in the burst mode is shown in the two upper panels of Figure 2. During this time RBSP-B was in the morning sector in the Southern Hemisphere and had the following coordinates: MLT ~5.1 hr, MLAT ~ −17.4°, and $L \sim 3$. The electron plasma frequency f_p corresponding to the measured electron density was 379.5 kHz, and the electron cyclotron frequency f_c was 51.4 kHz. Both electric and magnetic receivers registered whistlers, sometimes with their echoes, and VLF noise below 6 kHz. The most intense whistlers were registered at about 19:24 UT, first a fractional hop whistler at 19:23:57 UT, which came from the Southern Hemisphere, and then three echo signals, after which a decrease in the VLF noise intensity below 6 kHz can be observed (see Figure 3b). Minimum intensity of the VLF noise was observed ~20 s after the first reflected whistler. F2 F3

Before proceeding with the description of the wave phenomenon under consideration, an important remark is in order. Following the original paper by Gail and Carpenter (1984), we use VLF noise and VLF hiss as equivalent terms for the emission being suppressed by whistler trains. As this emission is observed inside the plasmasphere, we should clarify the relation between this emission and the plasmaspheric hiss. The latter is usually understood as the emission in the frequency band from hundred(s) Hz to several kHz, with maximum spectral intensity below 1 kHz (see, e.g., Summers et al., 2014, and references therein). In a sense, the VLF hiss under discussion may be considered as the higher-frequency part of plasmaspheric hiss, with its specific features, namely, noise-like spectrum, predominantly parallel wave normal vectors, the Poynting vectors directed from the equator, and relatively low intensity as compared to that at lower frequencies. Thus, for instance, the maximum power spectral density of the wave magnetic filed for the plasmaspheric hiss at the frequency 500 Hz was about $8 \cdot 10^6$ nT^2 Hz^1, while the power spectral density of the VLF hiss at the frequencies of (4–6) kHz was about 2 orders of magnitude lower.

Suppression of the noise intensity by whistler can be clearly seen from Figure 3b which shows electric field spectral density in three frequency bands centered on 3988, 5020, and 5623 Hz in the time interval 19:20–19:28 UT. Three distinct spikes of spectral amplitude, which we associate with multihop whistlers (marked by "w" in the figure), followed by decrease in the noise amplitude are clearly seen. Minimum values of the noise intensity marked by arrows are observed ~(15–30) s after whistlers.

Figure 3a shows cold plasma density (Kurth et al., 2015) along the satellite trajectory, which smoothly increases between 19:21 and 19:24 UT, then remains almost constant and then slightly decreases after 19:27:30 UT. The amplitudes of whistlers and VLF noise also increase till 19:24 UT, whereupon intense whistlers are not observed, while the amplitude of noise slowly decreases. Simultaneous increase of the cold plasma density and VLF wave amplitudes (both of whistlers and VLF noise) may be related to ducting of whistler waves by density gradient of the cold plasma (Inan & Bell, 1977; Semenova & Trakhtengerts, 1980).

Ducted propagation of whistlers and VLF noise is confirmed by multicomponent analysis of VLF waves. Lower panels of Figure 2 show (c) planarity of the wave magnetic field (Santolík et al., 2002), (d) wave normal angle (Santolík et al., 2003), and (e) a spectral estimate of a polar angle of Poynting vector with respect to the ambient magnetic field (Santolík et al., 2010). One can see that fractional hop whistler propagates

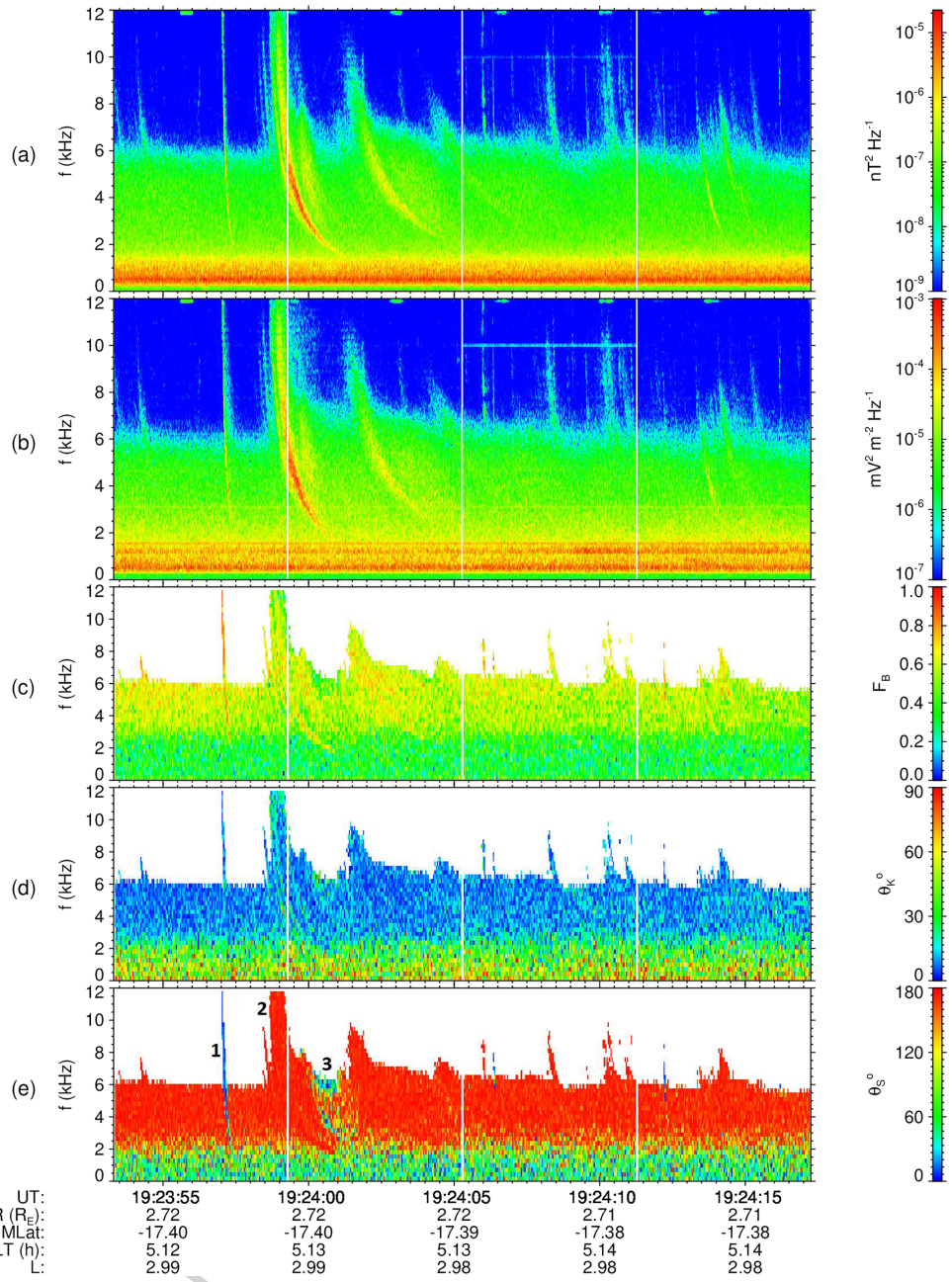

Figure 2. Dynamic spectra of VLF emission computed from RBSP-B waveform data for wave event observed on 22 December 2014. The sum of the power spectral densities of three orthogonal (a) magnetic and (b) electric components. (c–e). The results of multicomponent analysis of VLF wave measurements by RBSP-B on 22 December 2014 (see text for explanation of the displayed quantities).

toward the Northern Hemisphere, while further multihop whistlers propagate by turns toward the Southern and Northern Hemisphere. At the same time, VLF noise propagates toward the Southern Hemisphere. An important result that follows from the multicomponent analysis consists in that both whistlers and VLF noise have small wave normal angles. This suggests that the observed multihop whistlers propagate in ducted mode and that VLF noise is most probably generated at the equator.

To check the assumption that resonant interaction of energetic electrons with multihop whistlers changes their distribution in such a way that the free energy of the distribution is decreased, leading to the corresponding decrease in the growth rate, we have calculated the growth rates for parallel-propagating whistler waves using the data from MagEIS instrument on RBSP-B (Blake et al., 2013). This growth rate is determined

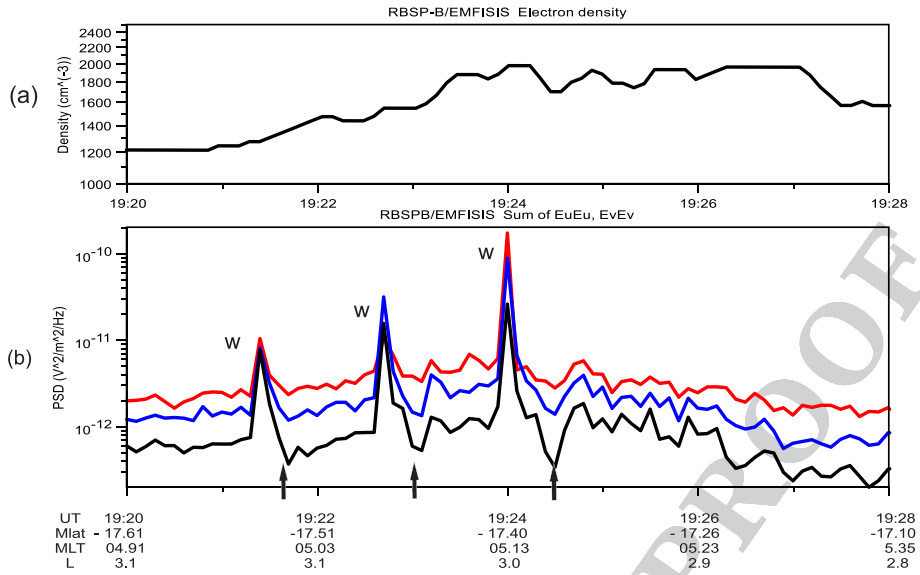

Figure 3. (a) Cold plasma density measured by RBSP-B. (b) Power spectral densities of electric field fluctuations as a function of time observed by RBSP-B in the frequency bands 3758–4218 Hz (red line), 4730–5309 Hz (blue line), and 5309–5957 Hz (black line).

by the expression given in Sagdeev and Shafranov (1961). Assuming that electron distribution function determining the growth rate is the function of particle kinetic energy $w = mv^2/2$ and magnetic momentum $\mu = mv_\perp^2/2\omega_c$ (m, v, $v_\perp$ are electron mass and total and transverse velocities, respectively, and ω_c is electron cyclotron frequency), this expression takes the form:

$$\gamma_L = \omega \frac{8\pi^3 e^2 \omega_c(\omega_c - \omega)}{m^2 k^3 c^2} \int_0^\infty d\mu f_0'(\mu)\mu \ . \tag{2}$$

Here ω is the wave angular frequency, k is the magnitude of the wave normal vector, e is the magnitude of electron charge, c is the speed of light, and

$$f_0'(\mu) = \left(\frac{\partial f_0}{\partial \mu} + \omega \frac{\partial f_0}{\partial w} \right)_{w = mv_R^2/2 + \mu\omega_c} , \tag{3}$$

where

$$v_R = \frac{\omega - \omega_c}{k} \tag{4}$$

is the resonance velocity at the first cyclotron resonance, the only one that exists at parallel propagation. As it is indicated above, after taking the derivatives in (3), particle parallel velocity is equated to v_R, so that the combined derivative (3) becomes a function of the magnetic momentum.

Electron distribution function that enters the above relations is determined from the measured electron differential flux by the relation (Cornilleau-Wehrlin et al., 1985):

$$f(w, \mu) \simeq 1.67 \cdot 10^{-37} \frac{J}{W} \ . \tag{5}$$

Relation (5) determines the electron distribution function in CGS system of units, used in the paper, through the measured differential electron flux J expressed in practical units, that is, $(cm^{-2} \cdot s^{-1} \cdot sr^{-1} \cdot keV^{-1})$ and the particle energy in keV denoted by W. We should underline that, no matter in which variables the distribution function is expressed, it is always equal to particle density in the phase space $(\mathbf{r}, \mathbf{v})$. Normalized growth rates calculated from RBSP-B data for two moments of time (before and after strong whistler events) are shown in Figure 4 as functions of frequency normalized to local electron cyclotron frequencies, which at that moments of time were equal to 43.85 and 49.03 kHz, respectively. We see that the decrease of growth rate after the series of three multihop whistlers is significant. Qualitative explanation of this result follows from the consideration in the next section. F4

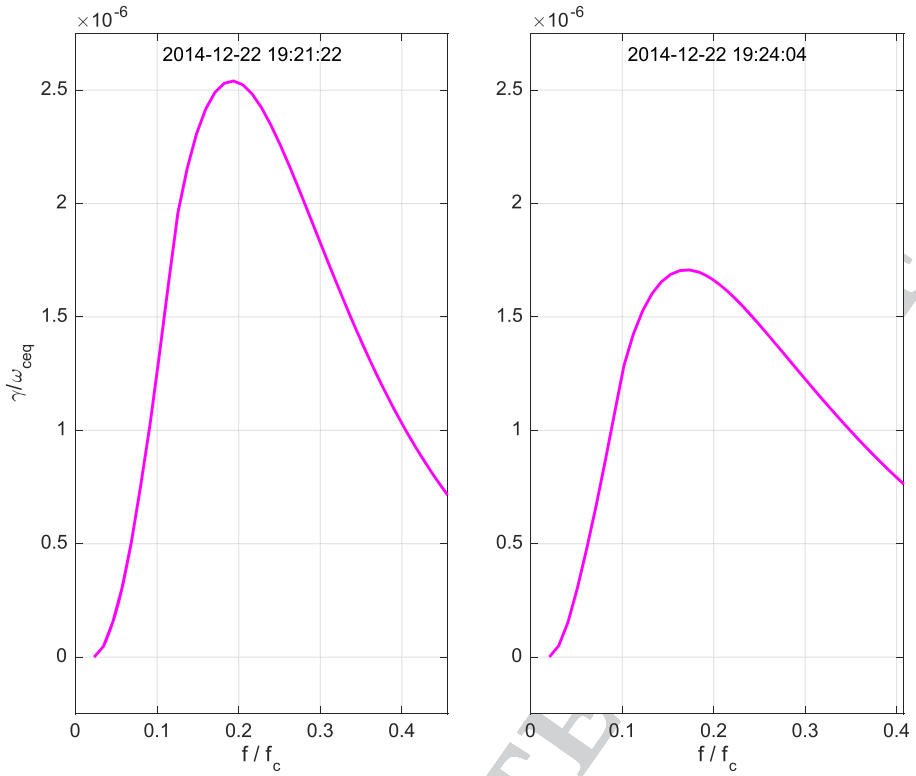

Figure 4. Normalized growth rate versus normalized frequency for parallel-propagating whistler mode waves calculated from RBSP-B measurements of electron fluxes by MagEIS instrument. Left and right panels display the normalized growth rate before and after the series of whistlers shown in Figure 3.

While the decrease in the growth rate related to strong whistler events is clearly seen in Figure 4, the unstable frequency band does not correspond to that of the equatorial VLF noise, and the magnitude of the growth rate is quite small. There are several reasons for these. First, the observed spectrum is determined not by the growth rate but rather by the amplification factor along the wave trajectory, as well as other factors, in particular, by the reflection coefficients at the mirror points. Second, the main contribution to the wave amplification factor comes from the near-equatorial region where the growth rate is largest and the group velocity is minimal. We presented the growth rates at the latitude $\sim -17.4°$ only for illustrative purposes, as we have in situ measurements of the particle distribution function in this region, to demonstrate the decrease of the growth rate after strong whistler echo train event. At the latitude $\sim -17.4°$ the loss cone is wider than at the equator, while the cyclotron frequency and, thus, the resonance velocity are larger. Due to these factors, outside the equator we should expect smaller values of the growth rate, but wider unstable frequency range, as the instability criterion is usually expressed in terms of the wave frequency normalized to cyclotron frequency and the effective anisotropy of the distribution function.

Unfortunately, we do not have measurements of the distribution function at the equator at the moments of time that we need, while the measurements outside the equator which we have do not permit to reconstruct the distribution function at the equator, since the particles with large perpendicular velocities that make the main contribution to the growth rate have mirror points close to the equator. That is why we have to rely upon direct calculation of the growth rate using the measured distribution function at the equator, at the same L-shell where the suppression phenomenon has been observed but at other moment of time. In particular, during the previous turnover, at 10:13:59, RBSP-B crossed the equatorial region exactly at $L = 3$, and we used the measurements of hot and cold plasma components to calculate the growth rate at the equator. This growth rate is shown in Figure 5. We see that at the equator, the growth rate is 1 order of magnitude larger than outside the equator, and the frequency of the growth rate maximum corresponds much better to the observed frequency band of VLF noise. F5

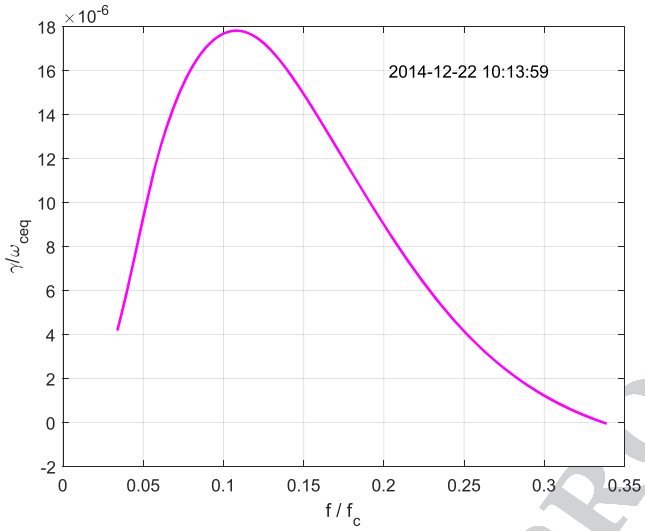

Figure 5. Normalized growth rate versus normalized frequency at the equator ($L = 3.09$, $\lambda = 0.75°$) calculated from electron fluxes measured by MagEIS instrument on RBSP-B on 22 December 2012, at 10:13:59 UT.

3. Qualitative Model of the VLF Noise Suppression by Whistlers

3.1. Main Assumptions of the Model

A general idea, which has been put forward by Helliwell et al. (1980) and Gail and Carpenter (1984) for explanation of the wave phenomenon under discussion, consists in the modification of the electron distribution function by whistler echo train in the way that reduces plasma instability causing the hiss generation. In the present study we follow up this idea and develop it into a qualitative model. A few assumptions suggested by observations that we use are as follows.

1. VLF noise is generated in the equatorial region of the magnetosphere by unstable plasma distribution and is characterized by a quasi-parallel direction of the wave normal vectors. The generation process is a subject of quasilinear theory, and thus, the growth rate is determined by the linear expression in which the unperturbed distribution function is replaced by varying in time phase-averaged distribution.
2. Whistler echo train causing the noise suppression propagates in ducted mode and can be described in the approximation of parallel propagation.
3. At the pre-event stage, the plasma is in a marginally unstable state, the upper frequency of the observed noise band corresponding to the boundary between unstable and stable frequency bands.
4. In the magnetospheric region, where the strong whistler interactions with resonant electrons responsible for the noise generation take place, the electromagnetic field of the whistler echo train can be represented as a sum of three wave packets bounded in space and time, with varying frequencies and wave numbers satisfying the local dispersion relation for parallel-propagating whistler mode waves. The frequency range of the causative whistler echo train overlaps the frequency band occupied by the suppressed noise.
5. While the generation of VLF hiss may be described in quasilinear approximation, that is, by the linear growth rate determined by the time-dependent distribution function, the strong whistler echo train changes the energetic particle distribution on the time scale much shorter than the quasilinear time.

3.2. Energetic Electron Motion in the Field of Whistler Echo Train

Since VLF noise suppression is usually observed after the second dispersed whistler trace, we will assume the wave field to consist of three wave packets: a fractional hop whistler originating from a lightning in the Southern Hemisphere (for the sake of definiteness) and two reflected whistlers, one from the Northern Hemisphere and one from the Southern Hemisphere, corresponding to the traces marked by numerals 1, 2, and 3 in the bottom panel of Figure 2. The first fractional hop whistler propagating from south to north and registered on the satellite in the Southern Hemisphere is marked by numeral 1. The trace corresponding to the wave packet reflected from the Northern Hemisphere is marked by numeral 2. The third trace corresponding to the wave packet reflected from the Southern hemisphere is marked by numeral 3. The waves that form this trace propagate to the north and are visible, although not very clearly, by blue color. The reason for this is twofold. First, the amplitude of the trace 3 is substantially lower than for the Trace 2 since the

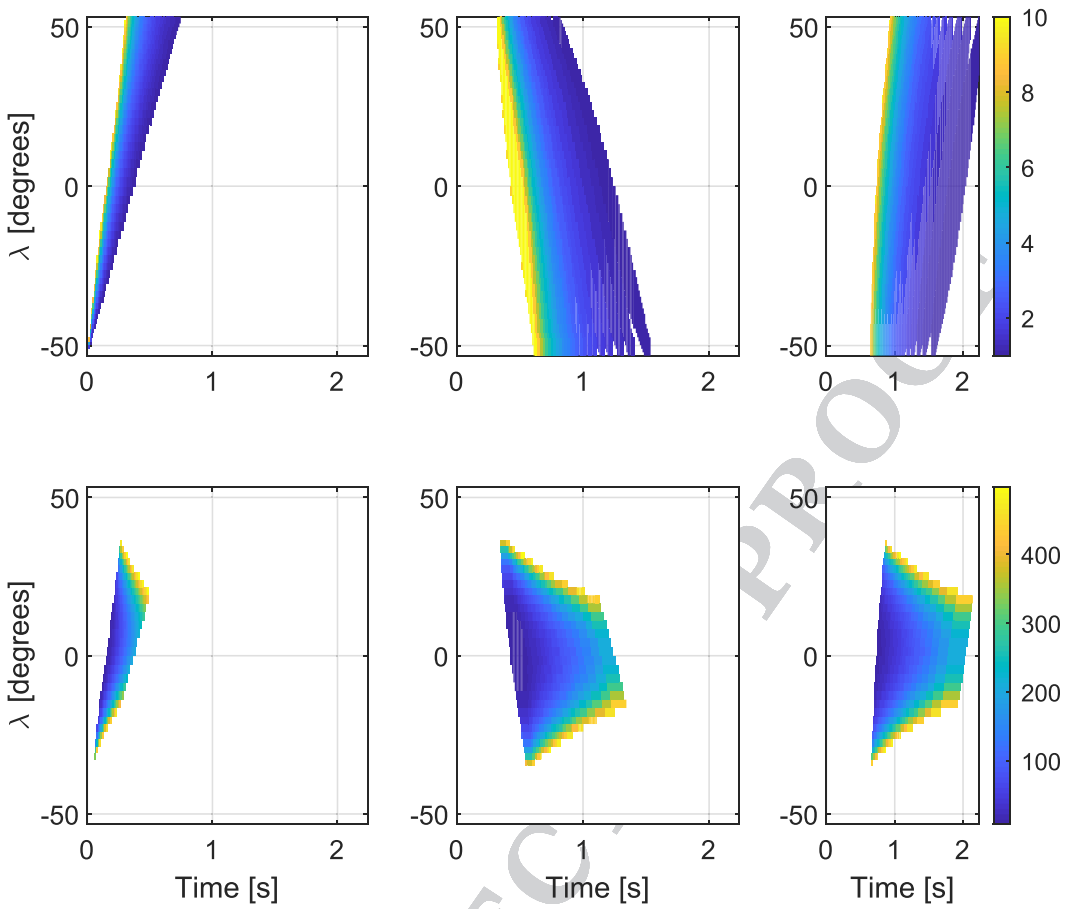

Figure 6. Upper panels. Frequency in kHz, color coded according to the color bar, in space-time domain of three wave packets corresponding to multihop whistlers: (left column) fractional hop whistler, (middle column) second hop whistler reflected from the ground in the Northern Hemisphere, and (right column) third hop whistler reflected from the ground in the Southern Hemisphere. Lower panels. Parallel resonance energy in keV, color coded according to color bar, in space-time domain for three wave packets corresponding to multihop whistlers. Only domains where the parallel resonance energy calculated according to nonrelativistic expression is below 500 keV are displayed.

waves that compose the former have not crossed the equatorial region where the essential cyclotron amplification takes place. Second, while Traces 1 and 2 are separated by double crossing the equator, where the time delay is most significant, the time delay between Traces 2 and 3 is smaller, since during this period the signal does not cross the equatorial region. The same is seen in Figure 6. While the Wave Packets 1 and 2 are well separated in space-time domain, the Wave Packets 2 and 3 strongly overlap. After the third trace, other whistlers reflected from the Northern Hemisphere and propagating to the south are seen in Figure 2. We do not discuss these traces and do not include them in numerical analysis of particle motion, since the effect of VLF noise suppression by whistlers is revealed after the first few traces.

Based on experimental observations, we will assume parallel propagation of all waves, which essentially simplifies the problem. In the case of parallel propagation, the wave field has only x and y components, transverse to the direction of wave propagation. Thus, we will write the wave electric field in the form

$$E_x(z,t) = -\sum_i E_{0i}(z,t)\cos\Psi_i(z,t) \quad E_y = \sum_i E_{0i}(z,t)\sin\Psi_i(z,t)\ ; \quad (i=1,2,3)\ , \tag{6}$$

where z is the coordinate along the ambient magnetic field and $E_{0i}(z,t)$ and $\Psi_i(z,t)$ are amplitudes and phases of the ith wave packet. In the following numerical calculations, we will not consider space-time variation of the wave amplitudes but will put them equal to 8 mV m^{-1} wherever the wave packets exist. At the same time, we will use exact expressions for wave packet phases as they follow from the equations of geometrical optics (GO).

The wave frequency and the wave normal vector in each wave packet are determined in the usual way:

$$\omega_i(z,t) = -\frac{\partial \Psi_i(z,t)}{\partial t} \quad k_{zi}(z,t) \equiv k_i(z,t) = \frac{\partial \Psi_i(z,t)}{\partial z} \,. \tag{7}$$

In each wave packet, the wave frequency $\omega_i(z,t)$ and the wave normal vector $k_i(z,t)$ depend on both coordinate z and time t, but for each z and t they are related by the dispersion relation for parallel-propagating whistler mode waves, namely,

$$\frac{k^2(z,t)\,c^2}{\omega^2(z,t)} = 1 + \frac{\omega_p^2(z)}{\omega(z,t)[\omega_c(z) - \omega(z,t)]} \,, \tag{8}$$

where $\omega(z,t)$ and $k(z,t)$ are the frequency and the wave number defined above which depend on (z,t), $\omega_p(z)$ is electron plasma frequency that depends on z, and $\omega_c(z)$ is, as before, the electron cyclotron frequency which also depends on z. The wave frequency in each wave packet calculated from the equations of GO under assumption of parallel propagation is shown in the three upper panels of Figure 6. For given frequency $\omega(z,t)$ and coordinate z, the wave number $k(z,t)$, up to its sign, is determined by (8). For the first and the third wave packets $k(z,t) > 0$, while for the second wave packet $k(z,t) < 0$. In order to find these quantities, we solved the equations of GO in the approximation of parallel propagation for 46 narrow band wave packets, starting at the height of 500 km in the Southern Hemisphere on L-shell equal to 3. For all of these wave packets, the initial wave vectors were parallel to the ambient magnetic field at the starting point, while their magnitudes corresponded, according to the local dispersion relation, to the frequencies in the range 1–10 kHz. We followed the solution of GO equations until the fast propagating 10 kHz wave reached the height of 500 km in the Northern Hemisphere after two reflections from the Northern and Sourthern Hemispheres. This forms three wide-band, space-time bounded wave packets that represent multihop whistlers or whistler echo train. In solution of the GO equations, we used the dipolar model of the ambient geomagnetic field and the gyrotropic model of the cold plasma density: $\omega_p^2 \propto \omega_c$ with the constant of proportionality that provides the ratio $\omega_p/\omega_c = 6$ at the equator on $L = 3$.

In nonrelativistic approximation, and for parallel-propagating whistler mode wave, the resonance between the wave and electron arises under condition $v_\parallel = (\omega - \omega_c)/k$. Correspondingly, electron resonance parallel energy in keV, with the account of (8), is given by

$$w_{\parallel \mathrm{res}}(z,t) \equiv \frac{m[\omega(z,t) - \omega_c(z)]^2}{2k^2(z,t)} \frac{1}{\mathrm{keV}} \simeq 256 \cdot \frac{[\omega_c(z) - \omega(z,t)]^3}{\omega(z,t)\omega_p^2(z)} \,, \tag{9}$$

where $\mathrm{keV} = 1.6 \cdot 10^{-9}$. The quantity $w_{\parallel \mathrm{res}}(z,t)$ in space-time domains where the multihop whistlers exist is shown in the three bottom panels of Figure 6.

The wave electric field in the form (6) corresponds to right-hand polarization with respect to the ambient magnetic field independently of the sign of wave number k, that is, of the direction of the wave propagation. In our case, k_1 and k_3 are positive, while k_2 is negative. The wave magnetic field can be found from the wave electric field (6) using the Faraday induction law.

In the absence of the wave field, particle kinetic energy w and magnetic momentum μ are conserved, and the particle motion can be described by the equations that follow from the unperturbed Hamiltonian

$$H_0 = \frac{p_\parallel^2}{2} + \mu\omega_c(z) \,, \tag{10}$$

where canonically conjugated variables are $(p_\parallel, z)$ and (μ, φ) and where φ is the particle gyrophase. Transverse components of electron velocity are expressed in canonical variables as follows:

$$v_x = \sqrt{\frac{2\mu\omega_c(z)}{m}} \cos\varphi \,; \quad v_y = \sqrt{\frac{2\mu\omega_c(z)}{m}} \sin\varphi \,. \tag{11}$$

We now write the variation of electron kinetic energy due to interaction with the whistler echo train:

$$\frac{\mathrm{d}w}{\mathrm{d}t} \equiv -e\mathbf{E}\mathbf{v} = e\sqrt{\frac{2\mu\omega_c(z)}{m}} \sum_i E_{0i} \cos[\Psi_i(z,t) + \varphi] \,, \tag{12}$$

where $-e$ is electron charge. As has been shown by Shklyar and Matsumoto (2009), for resonant particles, the rate of energy variation coincides with partial derivative of the interaction Hamiltonian with respect to time. Taking this into account, and making use of (10), we come to the expression for the total Hamiltonian of the problem in the form

$$H = \frac{p_\parallel^2}{2} + \mu\omega_c(z) - e\sqrt{\frac{2\mu\omega_c(z)}{m}} \sum_i \frac{E_{0i}}{\omega_i(z,t)} \sin[\Psi_i(z,t) + \varphi] \,. \tag{13}$$

The equations of motion which follow from the Hamiltonian (13) have the form

$$\frac{dz}{dt} = \frac{p_\parallel}{m} \,; \quad \frac{dp_\parallel}{dt} = -\mu\frac{d\omega_c}{dz} + e\sqrt{\frac{2\mu\omega_c(z)}{m}} \sum_i \frac{E_{0i}k_i(z,t)}{\omega_i(z,t)} \cos[\Psi_i(z,t) + \varphi] \,;$$
$$\frac{d\varphi}{dt} = \omega_c(z) - e\sqrt{\frac{\omega_c(z)}{2\mu m}} \sum_i \frac{E_{0i}}{\omega_i(z,t)} \sin[\Psi_i(z,t) + \varphi] \,; \frac{d\mu}{dt} = e\sqrt{\frac{2\mu\omega_c(z)}{m}} \sum_i \frac{E_{0i}}{\omega_i(z,t)} \cos[\Psi_i(z,t) + \varphi] \,. \tag{14}$$

While we have taken into account the derivative of cyclotron frequency with respect to z in the equation for $p_\parallel$ that originates from the unperturbed Hamiltonian, we have neglected the derivatives with respect to z of slowly varying quantities $\omega_i(z,t), k_i(z,t)$ and E_{0i} in the interaction Hamiltonian that contains wave amplitudes E_{0i} as the factors. This is valid under conditions of applicability of GO $k_i\mathcal{L} \gg 1$, where $\mathcal{L}$ is the characteristic scale of plasma inhomogeneity. We should stress that neglecting the *derivatives* of the abovementioned quantities with respect to z in the equation for $p_\parallel$ by no means imply that we treat them as constant; we do take into account their variation in space and time along the particle trajectory.

In the set of equation (14), the quantity φ is an unknown function, while the quantities $\Psi_i(z,t)$ should be considered as known ones. However, the equations of GO from which the quantities $\Psi_i(z,t)$ should be found define first of all their derivatives, that is, the quantities $\omega_i(z,t)$ and $k_i(z,t)$. That is why, in the equations of motion (14), it is convenient to use quantities $\zeta_i = \Psi_i(z,t) + \varphi$ as new unknown functions, since the function φ enters the equations of motion only in combinations ζ_i. Thus, instead of equation for φ and equations for $\Psi_i(z,t)$, it is more convenient to use the equations for ζ_i, which follow from the definitions given above and the equation for φ:

$$\frac{d\zeta_i}{dt} = \frac{k_i(z,t)p_\parallel}{m} - \omega_i(z,t) + \omega_c(z) - e\sqrt{\frac{\omega_c(z)}{2\mu m}} \sum_j \frac{E_{0j}}{\omega_j(z,t)} \sin\zeta_j \,. \tag{15}$$

In these equations, the quantities $k_i(z,t)$ and $\omega_i(z,t)$ are the functions that are found directly from the equations of GO.

We will underline the difference between the equations of motion written above and those used when considering resonant particle dynamics in one wave packet on a short time scale, that is, on the time scale of crossing one cyclotron resonance (Nunn, 1971 see also Demekhov et al., 2006; Karpman et al., 1975; Shklyar & Matsumoto, 2009). In the latter case it is often convenient to choose the sum of the wave phase and particle gyrophase as a new dependent variable (phase) and the derivative of this quantity with respect to time, which is proportional to the deviation of particle parallel velocity from the resonant value, as the second variable (momentum). Then the equation for this momentum contains the derivatives of the quantities $\omega_c(z)$, $\omega_i(z,t)$, and $k_i(z,t)$ in an evident form. This procedure is not appropriate in our case. First, we have three phases ζ_i instead of one. Second, we consider particle dynamics on a large time scale that includes many bounce oscillations and many crossings of cyclotron resonances inside three wave packets. That is why we need to follow the variations of three phases (equation (15)), as well as the variation of parallel coordinate z, parallel momentum $p_\parallel$, and the magnetic momentum μ (equation (14)), while the equation for particle gyrophase φ is included in the equation (15). In fact, we also follow the variation of particle kinetic energy according to equation (12). In all these equations we take into account the dependencies of quantities entering these equations on z and t, as it is indicated in the equations.

The solutions of the set of equation (14) for three particles are shown in Figures 7 and 8. Upper panels of Figure 7 show the variations of latitude, normalized parallel velocity, and normalized magnetic momentum along the particle trajectories. We see that, on large time scale, the particles bounce oscillates between

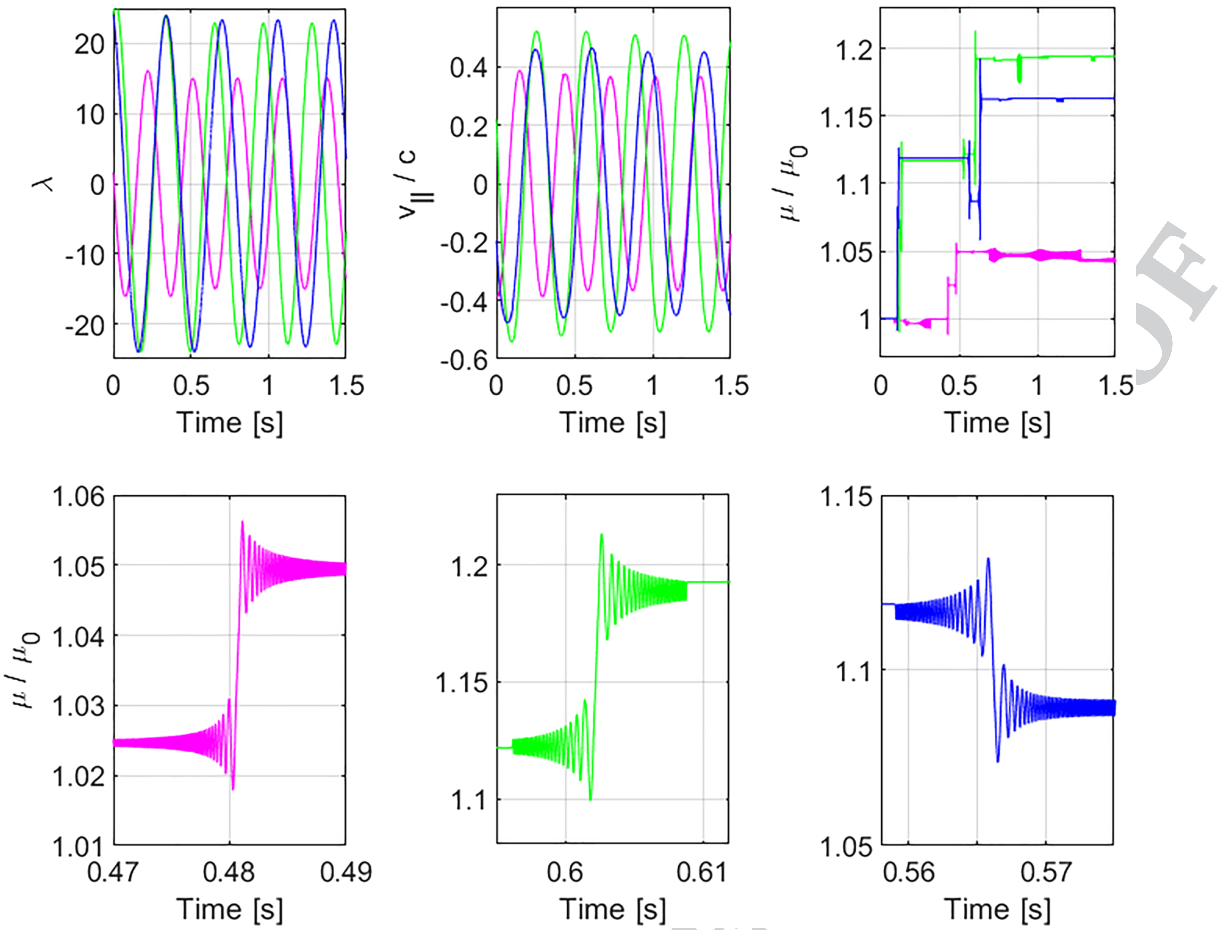

Figure 7. Time variations of particle latitude λ, longitudinal velocity $v_{\|}$, and magnetic momentum μ normalized to its initial value μ_0, for three particles shown in magenta, green, and blue, along their trajectories in the field of multihop whistlers and the ambient geomagnetic field. Initial parameters of the particles are, respectively, as follows: λ_0=(1.55°, 24.05°, 24.05°); $v_{\|0}$ =(−0.39c, 0.22c, −0.19c); $\zeta_{1,0} = \zeta_{2,0} = \zeta_{3,0}$ = (6.02rad, 0.99rad, 0.99rad); $\mu_0\omega_{ceq}$ = (0.18, 0.11, 0.09) mc^2; w_0 = (0.26, 0.26, 0.20) mc^2. Particles move along $L = 3$ where electron cyclotron frequency at the equator $\omega_{ceq} = 2.02 \cdot 10^5$rad.

mirror points occasionally experiencing resonant impacts from multihop whistlers. These impacts change the particle energy and magnetic momentum, the variations taking place during a very short time as compared to bounce period. One of such impacts for each particle is zoomed in the bottom panels of the figure. As one can see from Figure 8, which displays the variations of particle energy (upper panel), each impact corresponds to stationary phase point in one of the wave packets, that is, to the moment at which one of the derivatives $d\zeta_i/dt$ shown in three lower panels turns to zero. We suggest that random jumps of electron energy and magnetic momentum in the course of interaction with multihop whistlers cause particle diffusion in the phase space, which leads to a decrease in free energy of the unstable distribution and the corresponding decrease of the growth rate.

For quantitative estimation of the suggested mechanism, we have calculated the average variation squared, during the duration of the whistler echo train $\Delta t = 2.24$ s, of magnetic momentum for 100 particles with a characteristic initial energy $w_c = 132$ keV and a characteristic magnetic momentum μ_c such that $\mu_c\omega_{ceq} = 56.6$ keV, uniformly distributed over gyrophases and the accessible range of initial latitudes on $L = 3$. These determine the particle diffusion coefficient $D_{\mu\mu}$ according to the relation

$$D_{\mu\mu} = \frac{\overline{(\Delta\mu)^2}}{2\Delta t}\,, \tag{16}$$

where the overline means the average over the time Δt. For the parameters of the model described above, the calculations give $\overline{(\Delta\mu)^2}/\mu_c^2 = 0.072$, so that $D_{\mu\mu}/\mu_c^2 \simeq 0.016$ s^{-1}.

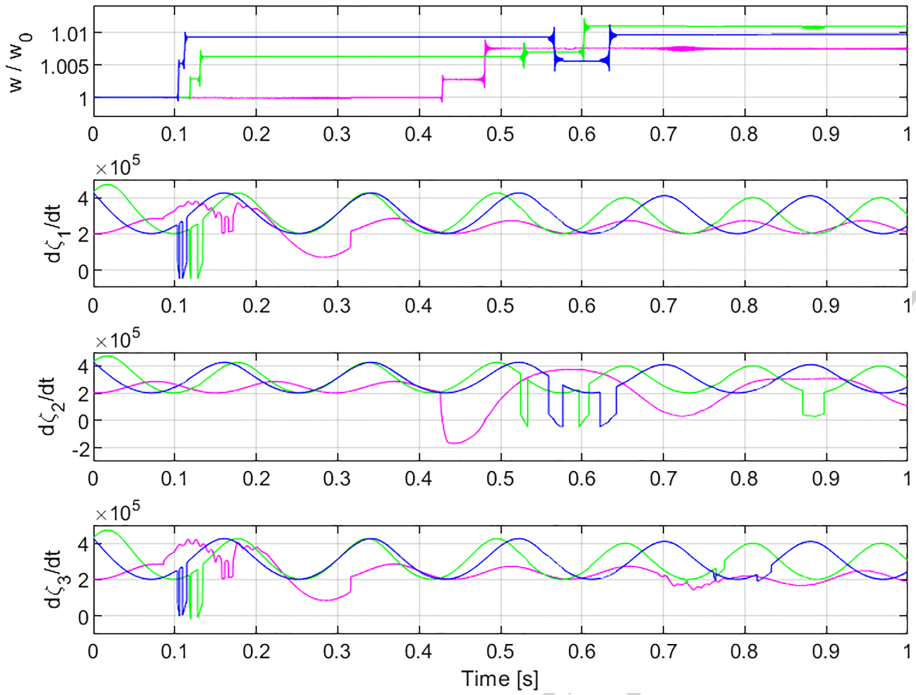

Figure 8. Time variations of particle kinetic energies w normalized to initial values and derivatives of the phases of three wave packets representing multihop whistlers. Initial conditions and color correspondence are the same as in Figure 7.

While the term "characteristic energy" just means a typical energy of energetic particles, the term "characteristic magnetic momentum" needs some explanation. We assume that plasma in the equatorial region is unstable. It means that the integral with respect to μ in (3) is positive. By the characteristic magnetic momentum, we understand the center of the region which makes the main contribution to the integral with respect to μ.

As is well known, for diffusion process $\overline{(\Delta\mu)^2} \propto \Delta t$, thus, the diffusion coefficient $D_{\mu\mu}$ does not depend on time Δt for which it has been calculated, since with increasing Δt, the quantity $\overline{(\Delta\mu)^2}$ increases proportionally. The characteristic diffusion time t_D is determined as the time for which $\overline{(\Delta\mu)^2} \sim \mu_c^2$. During this time, diffusion covers the entire region in the phase space which makes the main contribution to the growth rate, and we should expect its essential decrease after $t \sim t_D$. Substitution t_D for Δt and μ_c^2 for $\overline{(\Delta\mu)^2}$ in (16) gives

$$t_D = \frac{\mu_c^2}{2D_{\mu\mu}} \,. \tag{17}$$

Using the figures given above, we obtain the characteristic diffusion time $t_D \simeq 31$ s, which also provides an estimation for the relaxation time of unstable plasma distribution.

4. Concluding Remarks

We have presented experimental evidences of VLF noise suppression by strong whistlers which is observed on VLF spectrograms obtained at Kannoslehto ground station, after cleaning them from sferics, as well as on spectrograms obtained on the Van Allen Probe B satellite. The investigation of suppression effect based on satellite wave and particle measurements has been performed for the first time.

The idea that we use to explain this phenomenon can be traced back to early works by Helliwell et al. (1980) and Gail and Carpenter (1984). It consists in the assumption that, due to interaction with strong whistlers, the unstable electron distribution is modified in such a way that decreases the instability threshold. This modification should first of all be revealed at the boundary of unstable band, as is indeed observed in experiment.

Our general approach to the problem of VLF noise suppression by whistlers consists in the following. According to observations, the emission above 2 kHz that we consider has an incoherent spectrum, with low spectral intensity as compared, for instance, to that below 1 kHz. The evolution of such a spectrum is a subject of quasilinear theory. One of the main concepts of this theory consists in that the growth rate which determines the evolution of this spectrum is determined by the linear growth rate, with the unperturbed distribution function replaced by the phase-averaged time-dependent distribution obtained from a diffusion equation in the phase space. This diffusion is a relatively slow process since the diffusion coefficients are proportional to spectral intensity which is assumed to be small and which is fulfilled in our case as has been mentioned above. In the quasilinear theory, there are no coherent effects, such as phase trapping by strong whistler echo train, of course. We suggest that in the presence of whistler echo train that brings these effects into play, the evolution of the distribution function determining the growth rate of VLF noise takes place much faster, which permits to explain the suppression effect.

To develop these ideas, we set forth a theory of electron resonant interaction with parallel-propagating multihop whistlers (whistler echo train). For the first time, we have derived and solved numerically the set of equations that describe electron motion in the field of three wave packets representing the multihop whistlers and the ambient inhomogeneous geomagnetic field. These equations take into account space-time variations of frequencies and wave vectors in the packets, as well as space-time boundedness of the wave packets. We have shown that resonant interaction with such wave packets leads to faster electron diffusion in the phase space. We suggest that this diffusion causes the modification of unstable electron distribution and is responsible for the suppression effect.

Although in a sense the VLF noise may be considered as an upper frequency part of plasmaspheric hiss, we should stress that the problem of VLF noise suppression by whistlers is related but by no means identical to the problem of plasmaspheric hiss origin (Bortnik et al., 2009; Nakamura et al., 2016; Omura et al., 2015), and in fact, the latter is out of the scope of the present paper.

Acknowledgments
This study was done in the frame of the Grant 294931 of the Academy of Sciences of Finland. D. R. S. and E. E. T. also acknowledge support from RFBR Grant 19-02-00179. O. S. and I. K. acknowledge support from Grants LTAUSA17070, GACR 17-07027S, and the Praemium Academiae award from the CAS. The authors thank the PI of EMFISIS instrument C. Kletzing and the PI of MagEIS instrument H. Spence of Van Allen Probes team for the use of the data which is available online (http://cdaweb.sci.gsfc.nasa.gov/istp_public/). SGO ELF-VLF quicklook plots are available online (http://www.sgo.fi/pub_vlf/).

References

Blake, J. B., Carranza, P. A., Claudepierre, S. G., Clemmons, J. H., Crain Jr. W. R., & Dotan, Y. (2013). The Magnetic Electron Ion Spectrometer (MagEIS) instruments aboard the Radiation Belt Storm Probes (RBSP) spacecraft. *Space Science Reviews*, *179*, 383–421. https://doi.org/10.1007/s11214-013-9991-8

Bortnik, J., Li, W., Thorne, R. M., Angelopoulos, V., Cully, C., & Bonnell, J. (2009). An observation linking the origin of plasmaspheric hiss to discrete chorus emissions. *Science*, *324*, 775–778. https://doi.org/10.1126/science.1171273

Cornilleau-Wehrlin, N., Solomon, J., Korth, A., & Kremser, G. (1985). Experimental study of the relationship between energetic electrons and ELF waves observed on board GEOS: A support to quasi-linear theory. *Journal of Geophysical Research*, *90*, 4141–4154.

Demekhov, A. G., Trakhtengerts, V. Y., Rycroft, M. J., & Nunn, D. (2006). Electron acceleration in the magnetosphere by whistler-mode waves of varying frequency. *Geomagnetism and Aeronomy*, *46*(6), 711–716.

Gail, W. B., & Carpenter, D. L. (1984). Whistler induced suppression of VLF noise. *Journal of Geophysical Research*, *89*(2), 1015–1022.

Helliwell, R. A., Mende, S. B., Doolittle, J. H., Armstrong, W. C., & Carpenter, D. L. (1980). Correlations between λ4278 optical emissions and VLF wave events observed at $L \sim 4$ in the Antarctic. *Journal of Geophysical Research*, *85*, 3376–3386.

Inan, U. S., & Bell, T. F. (1977). The plasmapause as a VLF wave guide. *Journal of Geophysical Research*, *82*(19), 2819–2827. https://doi.org/10.1029/JA082i019p02819

Karpman, V. I., Istomin, J. N., & Shklyar, D. R. (1975). Effects of nonlinear interaction of monochromatic waves with resonant particles in the inhomogeneous plasma. *Physica Scripta*, *11*, 278–284.

Kletzing, C. A., Kurth, W. S., Acuna, M., MacDowall, R. J., Torbert, R. B., & Averkamp, T. (2013). The Electric and Magnetic Field Instrument Suite and Integrated Science (EMFISIS) on RBSP. *Space Science Reviews*, *179*, 127–181. https://doi.org/10.1007/s11214-013-9993-6

Kurth, W. S., De Pascuale, S., Faden, J. B., Kletzing, C. A., Hospodarsky, G. B., Thaller, S., & Wygant, J. R. (2015). Electron densities inferred from plasma wave spectra obtained by the waves instrument on Van Allen Probes. *Journal of Geophysical Research: Space Physics*, *120*, 904–914. https://doi.org/10.1002/2014JA020857

Manninen, J., Turunen, T., Kleimenova, N., Rycroft, M., Gromova, L., & Sirviö, I. (2016). Unusually high frequency natural VLF radio emissions observed during daytime in Northern Finland. *Environmental Research Letters*, *11*, 124006. https://doi.org/10.1088/1748-9326/11/12/124006

Nakamura, S., Omura, Y., Summers, D., & Kletzing, C. A. (2016). Observational evidence of the nonlinear wave growth theory of plasmaspheric hiss. *Geophysical Research Letters*, *43*, 10,040–10,049. https://doi.org/10.1002/2016GL070333

Nunn, D. (1971). A theory of VLF emissions. *Planetary and Space Science*, *19*, 1141–1167.

Omura, Y., Nakamura, S., Kletzing, C. A., Summers, D., & Hikishima, M. (2015). Nonlinear wave growth theory of coherent hiss emissions in the plasmasphere. *Journal of Geophysical Research: Space Physics*, *120*, 7642–7657. https://doi.org/10.1002/2015JA021520

Ostapenko, A. A., Titova, E. E., Nickolaenko, A. P., Turunen, T., Manninen, J., & Raita, T. (2010). Characteristics of VLF atmospherics near the resonance frequency of the Earth-ionosphere waveguide 1.6-2.3 kHz by observations in the auroral region. *Annales Geophysicae*, *28*, 193–202.

Platino, M., Inan, U. S., Bell, T. F., Gurnett, D. A., Pickett, J. S., Canu, P., & Décréau, P. M. E. (2005). Whistlers observed by the Cluster spacecraft outside the plasmasphere. *Journal of Geophysical Research*, *110*, A03212. https://doi.org/10.1029/2004JA010730

Sagdeev, R. Z., & Shafranov, V. D. (1961). On the instability of a plasma with an anisotropic distribution of velocities in a magnetic field. *Soviet Physics Journal of Experimental and Theoretical Physics*, *12*, 130–132.

Santolík, O., Parrot, M., & Lefeuvre, F. (2003). Singular value decomposition methods for wave propagation analysis. *Radio Science*, *38*(1), 1010. https://doi.org/10.1029/2000RS002523

Santolík, O., Pickett, J. S., Gurnett, D. A., Menietti, J. D., Tsurutani, B. T., & Verkhoglyadova, O. (2010). Survey of Poynting flux of whistler mode chorus in the outer zone. *Journal of Geophysical Research*, *115*, A00F13. https://doi.org/10.1029/2009JA014925

Santolík, O., Pickett, J. S., Gurnett, D. A., & Storey, L. R. O. (2002). Magnetic component of narrow-band ion cyclotron waves in the auroral zone. *Journal of Geophysical Research*, *107*(A12), 1444. https://doi.org/10.1029/2001JA000146

Semenova, V. I., & Trakhtengerts, V. Y. (1980). On specific features of the LF waveguide propagation. *Geomagnetism and Aeronomy*, *20*(6), 1021–1027.

Shklyar, D., & Matsumoto, H. (2009). Oblique whistler-mode waves in the inhomogeneous magnetospheric plasma: Resonant interactions with energetic charged particles. *Surveys in geophysics*, *30*(2), 55–104.

Summers, D., Omura, Y., Nakamura, S., & Kletzing, C. A. (2014). Fine structure of plasmaspheric hiss. *Journal of Geophysical Research: Space Physics*, *119*, 9134–9149. https://doi.org/10.1002/2014JA020437